Available online at www.sciencedirect.com
SCIENCE DIRECT
Chemical Physics Letters 426 (2006) 393–397
CHEMICAL PHYSICS LETTERS
www.elsevier.com/locate/cplett

Crystalline nano-structures of Ga_2O_3 with herringbone morphology

R. Jalilian [a], M.M. Yazdanpanah [a], B.K. Pradhan [b], G.U. Sumanasekera [a,c,*]

[a] *ElectroOptics Research Institute and Nanotechnology Center, University of Louisville, KY 40292, United States*
[b] *Columbian Chemicals Co., Marietta, GA 30062, United States*
[c] *Department of Physics, University of Louisville, KY 40292, United States*

Received 9 May 2006; in final form 24 May 2006
Available online 3 June 2006

Abstract

Highly crystalline β-Ga_2O_3 nanowires with two morphologies have been synthesized through physical evaporation of Te doped GaAs powder in Ar atmosphere. Growth is not based on VLS mechanism due to absence of Te. S in place of Te resulted in similar nanostructures. Some of the nanowires exhibit herringbone morphology with presence of hexagonal crystallites in regular spacing along the nanowire axis. The crystal planes of the nanowires were found to be parallel to one of the facets of the crystallites implying these crystallites may serve as the nucleation centers for the growth. Other dominant nanowire morphology is single crystalline nanoribbons.

1. Introduction

Nanostructures have attracted a great deal of interest and attention due to their interesting fundamental properties and potential applications such as gas sensors, field emitters, and advanced optoelectronic devices [1–3]. Metal oxide crystals in particular exhibit unique structures and physico-chemical properties especially at nano meter scale. Variety of nanostructures with different geometrical morphologies including tubes (single or multiple), wires, rods, sheets, belts, diskettes have been synthesized in a predicable way. Functionalized oxide nanostructures are used as functional materials due to their tunable physical properties as a result of the presence of vacancies and mixed valence states. Ga_2O_3 is one of the mostly studied metal oxide nano structures [4]. β-Ga_2O_3 is a wide bandgap ($E_g = 4.9$ eV) compound with interesting electrical and optical properties. In order to grow Ga_2O_3 nanostructure, various methods including vapor–liquid–solid technique [5], arc-discharge method [6], physical deposition [7] and thermal evaporation of oxide powders at high temperature [8] have been employed. Also Ga_2O_3 nanobelts have been grown by heating the metallic Ga in a furnace through vapor–solid process [9] and by evaporating GaN powders at 100 °C in flowing oxygen [10]. Ho et al. have synthesized β-Ga_2O_3 nanoribbons by plasma immersion ion implantation of nitrogen into undoped GaAs and post-implant rapid thermal annealing [11]. Here, we present a novel process for the synthesis of β-Ga_2O_3 nanowires and nanoribbons with unique nano-structures by simple thermal decomposition of GaAs mixed with a chalcogenide such as Tellurium or Sulfur in the presence of trace amount of oxygen. Other growth methods have been conducted associating chalcogenide elements in the growth of nanostructures [12].

2. Experimental

Commercially available GaAs wafer doped with Te (with doping concentration of 5×10^{17} cm^{-3}) was ground and placed in a quartz boat. The boat was positioned in a horizontal quartz tube reactor inside a furnace and heated up to 1000 °C at a rate of 10 °C/min, and maintained at that temperature for ~1 h while Argon gas was flowing at a rate of 100 sccm. Then the reactor was cooled down to room temperature at a rate of 10 °C/min. The same process under identical experimental conditions was carried out for mixtures of individual components of pure

* Corresponding author. Fax: +1 502 852 0742.
E-mail address: gusuma01@gwise.louisville.edu (G.U. Sumanasekera).

0009-2614/$ - see front matter © 2006 Elsevier B.V. All rights reserved.
doi:10.1016/j.cplett.2006.05.089

GaAs and pure Te (S) (weight percent of GaAs: Te (S) was 0.9999:0.0001). In each process a white color web-like product was observed at the edges of the entire walls of the quartz boat (as shown in the inset of Fig. 1) while a black color product was collected on the cold part of the inner reactor wall in the down stream. The white color deposit on the quartz boat was found to be essentially nanostructures of Ga_2O_3 with unique morphologies. A controlled experiment using only GaAs powder (in the absence of Te or S) under identical growth conditions did not result in any nanowire growth. Further experiments were carried out with additional flow of pure oxygen during the growth to understand the effect of oxygen in the process. XRD, SEM, EDS, HRTEM, and Raman spectroscopy were used to characterize the material.

3. Results and discussion

Fig. 1 shows the X-ray diffraction (XRD) spectrum of the samples collected from different parts of the reactor; white color web-like structures at the edges of the boat (solid line) and black deposit on the inner walls of the reactor in the cold part at the down stream (dotted line). Also shown in the inset is the XRD pattern of the lump of black residue in the center of the boat. XRD pattern of the GaAs powder is also shown in the inset for comparison. The resulting spectra of the sample collected from the walls of the quartz boat matches very well with β-Ga_2O_3.

The diffraction peaks can be indexed to a monoclinic structure of β-Ga_2O_3 with lattice parameter $a = 5.8$ Å, $b = 3.04$ Å, $c = 12.23$ Å and $\beta_0 = 103.42°$. Most of the peaks are identified for various orientations as labeled in the spectrum for β-Ga_2O_3. No peak associated with other crystalline phases of gallium oxide was observed in the XRD spectrum.

This results suggested that the synthesized product only contains the crystalline phase of β-Ga_2O_3. We observed some differences in the intensity compared with the pattern of the bulk β-Ga_2O_3 powder, for which the most intense peaks correspond to (004), (104), and (200) orientations. In this study, the strongest peaks correspond to (200) and (006). This difference can be attributed to the one-dimensional nature of the structure. The XRD pattern of the residual material found in the center of the boat corresponds to that of bulk GaAs implying it consists of undecomposed GaAs. The XRD pattern for the material collected from the inner reactor wall seems to match with a mixture of GaAs and β-Ga_2O_3.

Fig. 2a shows the typical SEM image of the material obtained from the inner walls of the quartz boat after the synthesis using Te doped GaAs powder. Shown in the inset is the schematic diagram of the quartz boat with resulting products after the growth. Arrow shows the direction of Argon gas flow in the reactor. SEM micrograph reveals the presence of abundant Ga_2O_3 nanowires with a high aspect ratio of more than 10000. The diameter of these nanowires ranges between 10 and 100 nm with average diameter of ~ 50 nm. The length of nanowires ranges up to hundreds of micrometers. Energy-dispersive X-ray spectroscopy (EDX) results of a representative sample is shown in Fig. 2c. The spectrum exhibits dominant peaks of oxygen (at 0.5 keV), gallium (at 1.1, 9.3 and 10.2 keV), and carbon (at 0.3 keV). The intensity ratio of Ga and O peaks is consistent with the stoichiometry of Ga_2O_3. Interestingly, no traces of tellurium or sulfur were found in the EDX analysis suggesting the growth is not VLS based. Tel-

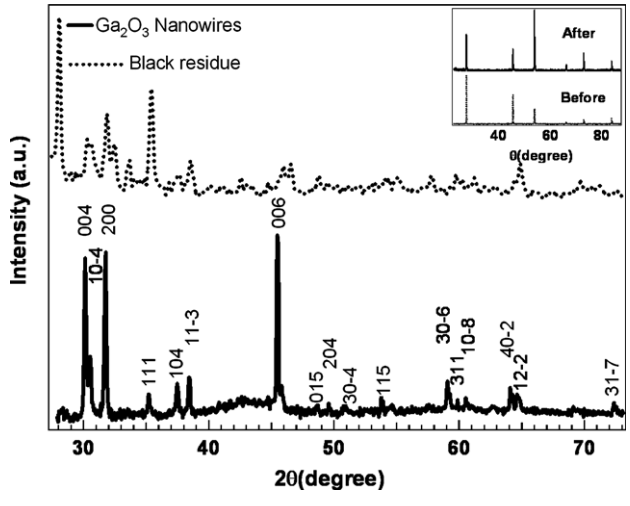

Fig. 1. XRD pattern of the samples collected from different parts of the reactor; white color web-like structures at the edges of the boat (solid line) and black deposit on the inner walls of the reactor wall in the cold part in the down stream (dotted line). Also shown in the inset is the XRD pattern of the lump of black residue in the center of the boat. XRD pattern of the GaAs powder is also shown in the inset for comparison.

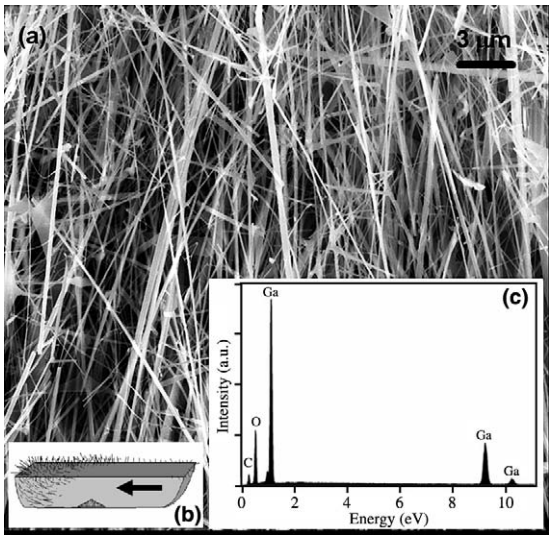

Fig. 2. (a) SEM image of the material obtained from the inner walls of the quartz boat synthesized using Te doped GaAs powder. (b) Shown in the inset is the schematic diagram of the quartz boat with resulting products after the growth. (c) EDX spectrum shows peaks corresponding to Ga, O and C.

lurium or sulfur do not play a role as a catalyst in typical VLS growth but rather act as a promoter in the process. Fig. 3 shows SEM micrographs of various Ga_2O_3 nanostructure morphologies resulted from (i) Te assisted growth: (a) comb-like structure (b) nanoribbon (c) herringbone structure (d) small diameter ($\sim$ 15 nm) nanowire, and (ii) S assisted growth: (e) larger size herringbone structured nanowires. The structures resulted in the presence of either Te or S show subtle differences.

Tellurium promoted experiments resulted in smaller size nanostructures while larger sheet-like structures were observed from S promoted growth. Herringbone structures obtained in both Te and S promoted growth have diameters ranging from 20 nm to 2 μm with length of tens of microns. The herringbone structures show the V-groove structure with an angle of $\sim 57°$ typical for most of them.

Fig. 4a shows a high-resolution TEM image along with a low-resolution image (inset) of an individual β-Ga_2O_3 nanowire. The width of this individual nanoribon is $\sim$ 25 nm. In HRTEM image of this nanowire, the lattice fringes of the (202) planes with a *d* spacing of 0.28 nm for monoclinic β-Ga_2O_3 can be observed clearly. It also indicates that the nanowire is single crystalline and the examined region is free from defects like dislocation or stacking faults, with no amorphous layer present. However, vacancy or interstitial defects may not be observed in HRTEM images. The growth axis for this nanowire is shown with an arrow, which is (010).

Fig. 5 shows TEM images of an individual Ga_2O_3 nanowire with a different morphology. Interestingly, this herringbone structures exhibit, an array of hexagonal crystals arranged in a regular spacing along the axis of the nanowire as in Fig. 5a, b. Fig. 5c shows that the hexagonal crystallites consist of crystal planes with spacing of $\sim$ 0.75 nm. Fig. 5d shows the selective area diffraction (SAD) pattern of the herringbone nanaowires indicating single crystallinity of Ga_2O_3. The HRTEM images shown in Fig. 5e reveal that the nanowires are single crystalline with lattice spacing of 0.35 nm. Interestingly, the crystalline planes of the herringbone structure are parallel to two of the facets of the hexagonal crystallites. It is believed that the Ga migrate after the decomposition of GaAs in the presence of Tellurium or Sulfur at elevated temperatures forming hexagonal Ga_2O_3 nanocrystals with the incorporation of oxygen present in the reactor or in the carrier gas or

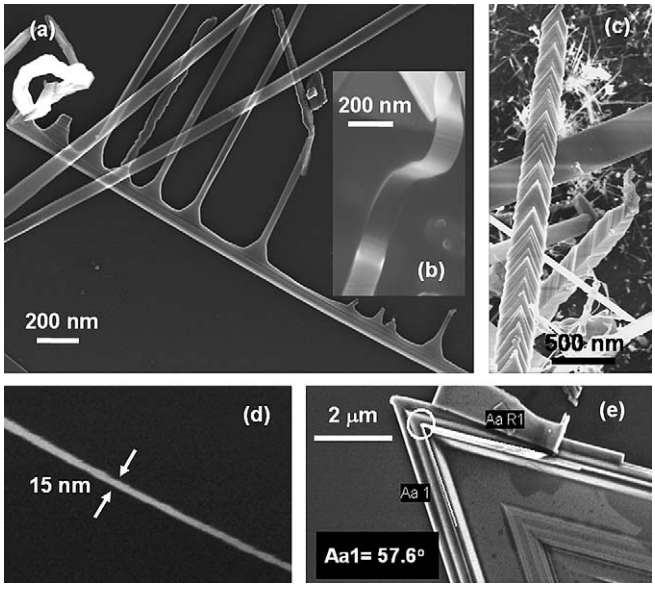

Fig. 3. SEM images of various Ga_2O_3 nanowire morphologies: (i) resulted from Te assisted growth; (a) comb-like structure, (b) nanoribbon, (c) herringbone structure, (d) small diameter ($\sim$ 15 nm) nanowire resulted from S assisted growth and (f) larger size of herringbone structure.

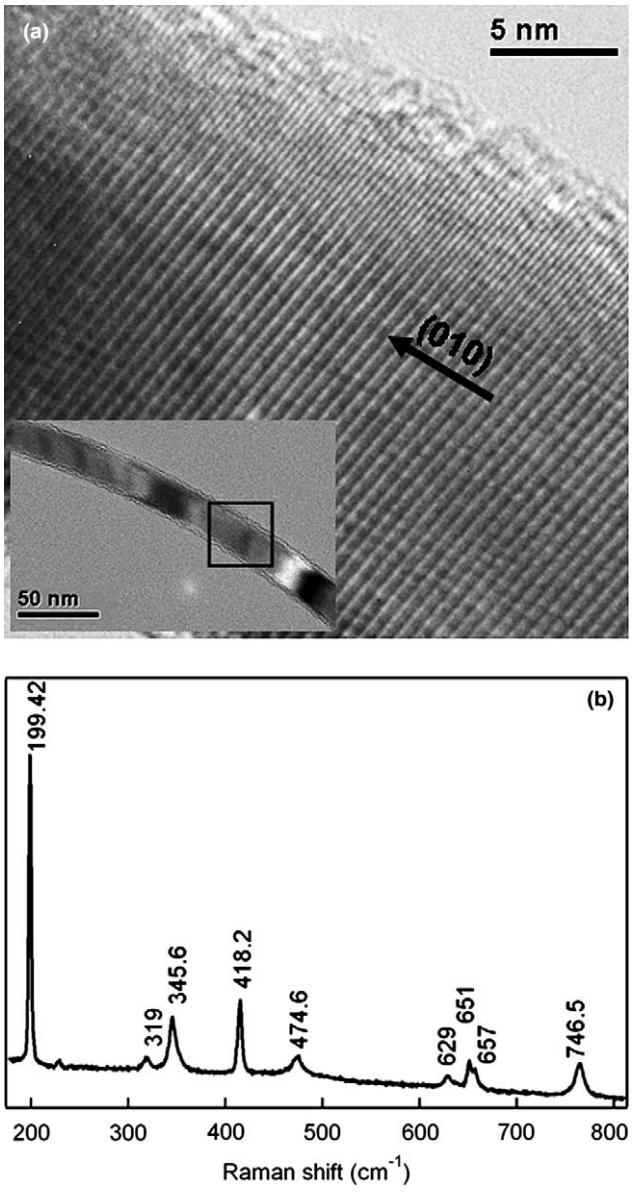

Fig. 4. (a) High-resolution TEM image of an individual nanowire showing structurally perfect surface. (inset) Low-resolution TEM image of an individual β-Ga_2O_3 nanowire. The image shows the nanowire with a uniform diameter. The lattice fringes of the (202) planes with a *d* spacing of $\sim$ 0.28 nm for monoclinic β-Ga2O3 can be observed clearly. The growth direction is (010) as indicated by the arrow. (b) Micro Raman spectrum of Ga_2O_3 nanostructures at room temperature.

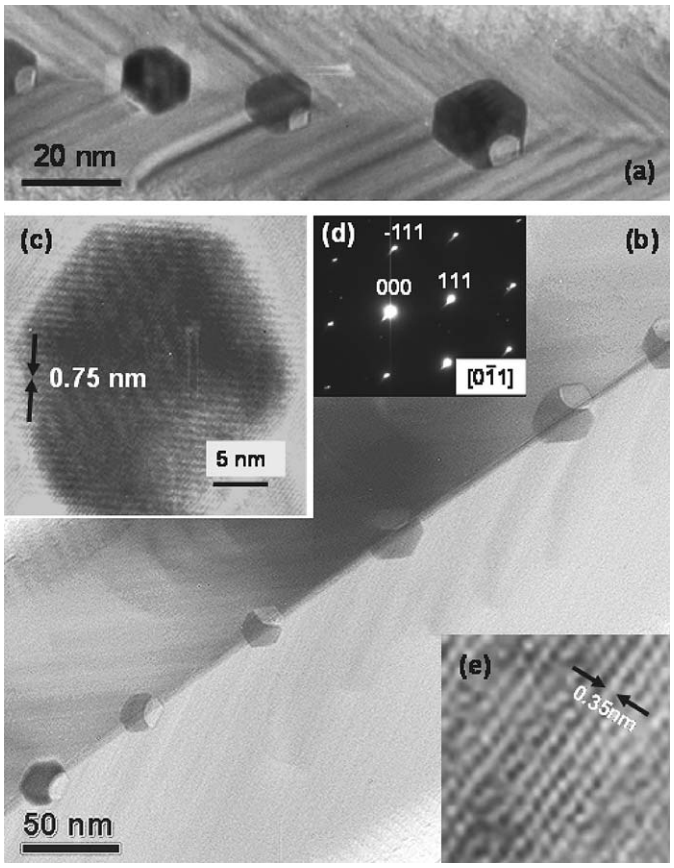

Fig. 5. TEM images of Ga_2O_3 herringbone structure; (a) and (b) the herringbone structured nanowire with an array of hexagonal crystallites arranged in a regular spacing along the axis of the nanowire (c) HRTEM image of a hexagonal crystallite consist of crystal planes with spacing of ~0.75 nm, (d) SAED pattern of a nanowire with a herringbone structure taken with [1–10] zone axis. The clear lattice fringes indicate a single crystal structure of the nanowire. (e) HRTEM image of the single crystalline nanowire with lattice spacing of 0.35 nm.

in the constituent materials. These nanocrystals in turn act as nucleation centers for the formation of Ga_2O_3 nanowires.

Chalcogens such as Te, S, and Se are typically used as dopants for GaAs in order to satisfy the dangling bonds on the GaAs surface [13]. It is also known the chalcogen treatment can lead to decrease in band bending [14]. This passivation can be attributed to the hetero-valent exchange of Arsenic with the chalcogen. This exchange reaction depends on the temperature and even at room temperature, some partial As–chalcogen exchange can take place. It is also known to form As–Te, As–S, and As–Se bonds [15,16]. At relatively lower temperatures these Arsenic chalcogenides are exhausted from the reactor whereas pure GaAs can only decompose at higher temperature and low pressures.

Fig. 4b shows the Raman spectrum of a representative Ga_2O_3 nanostructure obtained using a Renishaw Micro-Raman spectrometer with the laser excitation of 514.5 nm. Similar results were observed using 488 nm excitation laser (2 mW) and a 'HR460' Yobin–Yuan spectrometer.

Both sets of data are in excellent agreement with the vibrational modes of β-Ga_2O_3 structures confirming the high-quality of gallium oxide nanostructures. β-Ga_2O_3 belongs to the C_{2h}^3 space group, which predicts 27 sets of optical modes at $k = 0$ [17] given by $\Gamma = 10A_g + 5B_g + 8B_u + 4A_u$. Fifteen of them ($A_g$ and B_g) are Raman active and 12 of them (B_u and A_u) are IR active. Raman bands have been previously observed at 111, 114, 147, 169, 199, 318, 346, 353, 415, 475, 628, 651, 657, and 763 cm^{-1} in single crystals of β-Ga_2O_3 [18,19].

4. Conclusion

Ga_2O_3 nanowires were synthesized by simple thermal decomposition of GaAs powder at 1000 °C and subsequent oxidation of Gallium. Tellurium or sulfur was required for the growth of the nanostructures and believed to promote the reaction, but do not play a role as a catalyst in typical VLS growth as verified by the absence of traces of Te or S after the synthesis. The chalcogen exchanges As in GaAs by forming arsenic chacogenide that can be exhausted leaving Ga. Ga_2O_3 nanowires have single crystalline structure. The Herringbone structures exhibit single crystalline structure as observed by HRTEM image and single crystalline hexagonal crystallites are arranged in regular spacing along the central axis of the nanowire. These hexagonal crystallites are believed to act as the nucleation centers for the growth of the nanowires. Raman spectroscopy, EDX and XRD provide the evidence for the synthesized material to be β-Ga_2O_3. This method can be expanded to synthesize nanowires, nanoribbons, and nanosheets with varying sizes on a large scale and may find wide range of potential applications.

Acknowledgements

This study was partly sponsored by NASA cooperative agreement NCC5-571, US Army SMDC contract W9113M-04-C-0024 and US DOE (DE-FG02-00ER45832).

References

[1] W. Lu, J. Xiang, B.P. Timko, Y. Wu, C.M. Lieber, Adv. Mater. 16 (Sep 16) (2004).
[2] Z. Zhong, F. Qian, D. Wang, C.M. Lieber, NanoLetters 3 (2003) 343–346.
[3] D. Whang, S. Jin, Y. Wu, C.M. Lieber, NanoLetters 3 (2003) 1255–1259.
[4] D. Kohl, T. Ochs, W. Geyer, M. Fleischer, H. Meixner, Sensors Actuators B 59 (1999) 140–145.
[5] C.H. Liang, G.W. Meng, G.Z. Wang, Y.W. Wang, L.D. Zhang, Appl. Phys. Lett. 78 (2001) 3202.
[6] Y.H. Lee, Y.C. Choi, W.S. Kim, Y.S. Park, S.M. Lee, D.J. Bae, Adv. Mater. 12 (2000) 746.
[7] H.Z. Zhang, Y.C. Kong, Y.Z. Wang, X. Due, Z.G. Bai, J.J. Wang, D.P. Yu, Y. Ding, Q.L. Hang, S.Q. Feng, Solid State Commun. 109 (1999) 677.
[8] Z.W. Pan, Z.R. Dai, Z.L. Wang, Science 291 (2001) 1941.
[9] X. Xiang, C.B. Cao, Y.J. Guo, H.S. Zhu, Chem. Phys. Lett. 378 (2003) 660.

[10] J. Zhang, F. Jiang, Chem. Phys. 289 (2003) 243–249.
[11] H.P. Ho, K.C. Lo, K.Y. Fu, P.K. Chu, K.F. Li, K.W. Cheah, Chem. Phys. Lett. 382 (2003) 573.
[12] C.N.R. Rao, F.L. Deepak, G. Gundiah, A. Govindaraj, Prog. Solid State Chem. 31 (2003) 147.
[13] C.J. Sandroff, R.N. Nottenburg, J.C. Bishoff, R. Bhat, Appl. Phys. Lett. 51 (1987) 33.
[14] S. Takatani, T. Kikawa, M. Nakzawa, Phy. Rev. B 45 (1992) 8498.
[15] T. Scimeca, Y. Muramatsu, M. Oshima, H. Oigawa, Y. Nannichi, Phy. Rev. B 44 (1991) 12927.
[16] T. Scimeca, Y. Watanabe, R. Berrigan, M. Oshima, Phy. Rev. B 46 (1992) 10201.
[17] H.Z. Zhang, Y.C. Kong, Y.Z. Wang, X. Du, D.J. Bai, J.J. Wang, D.P. Yu, Y. Ding, Q.L. hang, S.Q. Feng, Solid State Commun. 109 (1999) 677.
[18] Y.C. Choi, W.S. Kim, Y.S. Park, S.M. Lee, D.J. Bae, Y.H. Lee, G.S. Park, W.B. Choi, N.S. Lee, J.M. Kim, Adv. Mater. 12 (2000) 746.
[19] L. Abello, B. Bochu, A. Gaskov, S. Koudryavtseva, G. Lucazeau, M. Roumyantseva, J. Solid State Chem. 135 (1998) 78.